Performance analysis of zero-IF MIMO OFDM transceivers with IQ imbalance

Performance Analysis of Zero-IF MIMO OFDM Transceivers with IQ Imbalance

Tim C. W. Schenk
Connectivity Systems and Networks department, Philips Research, Eindhoven, The Netherlands
Email: tim.schenk@philips.com

Erik R. Fledderus and Peter F. M. Smulders
Radiocommunication Chair, Eindhoven University of Technology, Eindhoven, The Netherlands
Email: {e.r.fledderus, p.f.m.smulders}@tue.nl

***Abstract*— This contribution analytically studies the influence of IQ mismatch on the performance of multiple-antenna orthogonal frequency division multiplexing (OFDM) systems based on the zero-IF architecture. First a system model for such a multiple-input multiple-output (MIMO) OFDM system experiencing both transmitter (TX) and receiver (RX) IQ imbalance is derived. This is used to obtain analytical expressions for the probability of error in symbol detection for MIMO OFDM systems in Rayleigh faded multipath channels. The derived results can be used to find matching specifications for the TX- and RX-branches for different multicarrier MIMO systems. It is concluded that in fading channels RX IQ imbalance is on average more destructive than TX IQ imbalance. Additionally, it is concluded that the addition of extra RX antennas is beneficial to reduce the dependence on *RX* IQ imbalance, but increases at the same time the impact of *TX* IQ imbalance.**

***Index Terms*— orthogonal frequency division multiplexing (OFDM), multiple-antenna systems, RF imperfections, IQ mismatch, fading channels, performance analysis**

I. Introduction

The advantages of multiple-input multiple-output orthogonal frequency division multiplexing (MIMO OFDM) as basis for next-generation high data-rate broadband wireless systems have been reported in many publications over the last few years [2–4]. Many challenges, however, remain in the efficient and low-cost implementation of these kind of systems, especially since they involve multiple radio front-ends. An obvious solution is the application of the *zero-IF* architecture [5] in both transmitter (TX) and receiver (RX), since it does not need external intermediate frequency (IF) filters and image rejection filters [6]. Instead, the image rejection is provided by the signal processing in the in-phase (I) and quadrature (Q) branch. Therefore, this architecture opens the door to monolithic integration of the analogue front-end and, thus, low-cost implementations.

This paper is based on "Performance impact of IQ mismatch in direct-conversion MIMO OFDM transceivers," by T. C. W. Schenk, E. R. Fledderus, and P. F. M. Smulders, which appeared in the Proceedings of the IEEE Radio and Wireless Symposium (RWS) 2007, Long Beach, USA, January 2007. [1] © 2007 IEEE.

This work was supported in part by the Dutch cooperative research project B4 BroadBand Radio@Hand (BTS01063).

The zero-IF transceiver architecture, also referred to as *homodyne* or *direct-conversion* architecture, however, has some disadvantages compared to more conventionally used heterodyne architectures. These disadvantages include DC offset through self-mixing, $1/f$-noise and increased IQ mismatch. This paper will focus on the latter impairment which is caused by mutual differences in the used components for frequency translation. These differences result in a phase and amplitude imbalance between the I and Q signals, an effect which we will refer to as *IQ imbalance* [7–10].

Previous contributions treat IQ imbalance in conventional single-input single-output (SISO) OFDM. They, however, mainly rely on simulation results and signal-to-interference ratio (SIR) derivations, see e.g. [7], [8], to study the performance impact. Although these results reveal the performance impact to some extend, they do not provide analytical expressions for the final system performance measure, i.e., the error rate. Recently, the probability of bit error for SISO OFDM systems impaired by RX IQ imbalance was analytically studied in [11]. Also, some recent papers, proposing digital compensation algorithms for IQ imbalance in MIMO OFDM systems [12–15], provide numerical results about the impact in MIMO OFDM systems. The influence of IQ imbalance on the SIR performance of a space-time coded single-carrier system was treated in [10].

This paper, which is an expanded version of [1], extends previous work by analytically studying the performance impact of both TX and RX IQ imbalance in a space division multiplexing (SDM)-based MIMO OFDM system. Symbol-error rate (SER) performance results are derived for Rayleigh fading channels. The results can be used to derive matching specifications for the TX- and RX-branches for next-generation MIMO OFDM systems. This paper extends [1] with a derivation of the influence of both TX and RX IQ mismatch on the MIMO OFDM system model, a more elaborated SER performance analysis and additional numerical and simulation results.

The outline of the paper is as follows. First the MIMO OFDM system model is introduced in Section II. Subsequently, Section III introduces the signal model for the

zero-IF architecture under perfect matching and IQ mismatch. Then the influence of IQ mismatch on the MIMO OFDM signal model is derived in Section IV. Expressions for the error in detection of the transmitted MIMO vector are obtained in Section V. These results are applied in Section VI to analytically develop novel expressions for the probability of symbol error for M-QAM signals. Section VII compares these analytical results with results from a numerical simulation study. Finally, conclusions are drawn in Section VIII.

II. MIMO OFDM SYSTEM MODELLING

Consider a MIMO OFDM system with N_t TX and N_r RX antennas, denoted here as a $N_\mathrm{t} \times N_\mathrm{r}$ system, applying $N_\mathrm{c} = 2K + 1$ subcarriers. The block diagram for the system is depicted in Fig. 1.

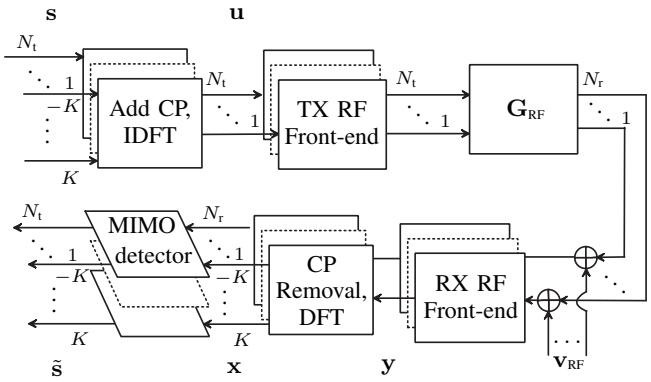

Figure 1. Multiple-antenna OFDM system model.

Let us define the mth $N_\mathrm{c}N_\mathrm{t}\times 1$ MIMO OFDM vector to be transmitted as $\mathbf{s}_m = \left[\mathbf{s}_{m,-K}^T, \ldots, \mathbf{s}_{m,K}^T\right]^T$, where $\mathbf{s}_{m,k}$ denotes the $N_\mathrm{t}\times 1$ frequency domain MIMO transmit vector for the kth subcarrier. The n_tth element of the subvector $\mathbf{s}_{m,k}$, corresponding to the n_tth TX branch, is denoted as s_{m,k,n_t}. The vector $\mathbf{s}_m$ is transformed to the time domain using the inverse discrete Fourier transform (IDFT), yielding

$$\mathbf{u}_m = (\boldsymbol{\Theta} \otimes \mathbf{I}_{N_\mathrm{t}})\, \check{\mathbf{u}}_m = \left(\boldsymbol{\Theta}\mathbf{F}^{-1} \otimes \mathbf{I}_{N_\mathrm{t}}\right) \mathbf{s}_m, \qquad (1)$$

where $\check{\mathbf{u}}_m = \left(\mathbf{F}^{-1} \otimes \mathbf{I}_{N_\mathrm{t}}\right) \mathbf{s}_m$, $\otimes$ denotes the Kronecker product, $\mathbf{F}$ is the $N_\mathrm{c}\times N_\mathrm{c}$ Fourier matrix, of which the (i,l)th element equals $\exp(-j2\pi\frac{i(l-(K+1))}{N_\mathrm{c}})$, and $\mathbf{I}_M$ represents the M dimensional identity matrix. A cyclic prefix (CP) is added to the signal $\check{\mathbf{u}}_m$ by multiplication with matrix $\boldsymbol{\Theta}$, which adds the last N_g elements of a vector on top of that vector. Here, N_g denotes the CP length for one TX antenna. We assume that by design N_g is at least equal to the channel impulse response (CIR) length, preventing inter-symbol interference (ISI).

The baseband transmit vector $\mathbf{u}_m$ is input to the N_t TX RF front-ends, which are used to up-convert the signals to be transmitted through the wireless channel, here modelled by $\mathbf{G}_{\mathrm{RF}}$. At the receiver, the signals obtained at the N_r antennas are down-converted using the N_r RX RF front-ends, yielding the mth received $N_\mathrm{c}N_\mathrm{r} \times 1$ complex baseband time domain vector $\mathbf{y}_m$, given by $\mathbf{y}_m = \left[\mathbf{y}_m^T(0), \ldots, \mathbf{y}_m^T(N_\mathrm{s}-1)\right]^T$. Here $\mathbf{y}_m(n)$ denotes the $N_\mathrm{r}\times 1$ received vector at sample instant n and N_s is the OFDM symbol length, given by $N_\mathrm{g} + N_\mathrm{c}$. The receiver noise is here denoted as $\mathbf{v}_{\mathrm{RF}}$ and its baseband equivalent is modelled as the $N_\mathrm{c}N_\mathrm{r} \times 1$ vector $\mathbf{v}_m$. The CP is removed by multiplication with $\boldsymbol{\Upsilon}$, which removes the first N_g elements of a vector. The received signal $\mathbf{y}_m$ is converted to the frequency domain using the discrete Fourier transform (DFT), which yields the $N_\mathrm{c}N_\mathrm{r}\times 1$ vector

$$\mathbf{x}_m = (\mathbf{F}\boldsymbol{\Upsilon} \otimes \mathbf{I}_{N_\mathrm{r}})(\mathbf{y}_m + \mathbf{v}_m). \qquad (2)$$

For perfect timing and frequency synchronisation and no front-end imperfection, the vector $\mathbf{x}_m$ can be written as function of the TX signal [4]

$$\mathbf{x}_m = \mathbf{H}\mathbf{s}_m + \mathbf{n}_m, \qquad (3)$$

where $\mathbf{n}_m$ is the frequency domain version of the noise vector $\mathbf{v}_m$ given by $(\mathbf{F}\boldsymbol{\Upsilon} \otimes \mathbf{I}_{N_\mathrm{r}})\mathbf{v}_m$. Here $\mathbf{H}$ denotes the $N_\mathrm{r}N_\mathrm{c}\times N_\mathrm{t}N_\mathrm{c}$ block diagonal frequency-domain channel given by $\mathrm{diag}(\mathbf{H}_{-K}, \ldots, \mathbf{H}_K)$, where $\mathbf{H}_k$ denotes the $N_\mathrm{r}\times N_\mathrm{t}$ MIMO channel matrix for the kth subcarrier. Note that we omitted the index m for the channel matrix, since we assume a quasi-static channel throughout this paper.

Due to the block-diagonal property of the channel matrix, the received signal vector for the kth subcarrier can also be written as

$$\mathbf{x}_{m,k} = \mathbf{H}_k\mathbf{s}_{m,k} + \mathbf{n}_{m,k}. \qquad (4)$$

Subsequently, MIMO detection can be applied per subcarrier to retrieve an estimate of the transmitted signal. In this paper we will restrict our analyses to SDM systems, where independent data streams are transmitted from the different TX branches. Also, we only consider zero-forcing (ZF) MIMO processing, where the estimate of the TX signal is found by multiplying the $\mathbf{x}_{m,k}$ with the inverse of a channel estimate $\tilde{\mathbf{H}}_k$, yielding

$$\tilde{\mathbf{s}}_{m,k} = \tilde{\mathbf{H}}_k^\dagger \mathbf{x}_{m,k} = \mathbf{s}_{m,k} + \boldsymbol{\varepsilon}_{m,k}, \qquad (5)$$

where † denotes the pseudo-inverse. For perfect channel knowledge, the error term $\boldsymbol{\varepsilon}_{m,k}$ is given by $\mathbf{H}_k^\dagger\mathbf{n}_{m,k}$.

III. ZERO-IF FRONT-END ARCHITECTURE

In this section we will now regard the zero-IF architectures used for frequency translation in the TX and RX. We will first consider the ideal architecture and subsequently consider the impact of IQ mismatch. Throughout this section we will apply, for notational convenience, the continuous time notation t, also for the digital time-discrete signals.

A. Perfect IQ matching

We first consider the up-conversion of the baseband signal $u_{n_\mathrm{t}}(t)$ in the n_tth TX branch, as illustrated schematically in Fig. 2(a). The real and imaginary part of the digital baseband signal $u_{n_\mathrm{r}}(t)$ are passed through the digital-to-analogue convertors (DACs). The signal is then up-converted to radio frequency (RF) f_c, using the quadrature mixing structure illustrated in the figure. The RF signal

is, before transmission through the channel, fed through the power amplifier (PA), which, in the analyses of this paper, we will assume to be perfect with unity gain.

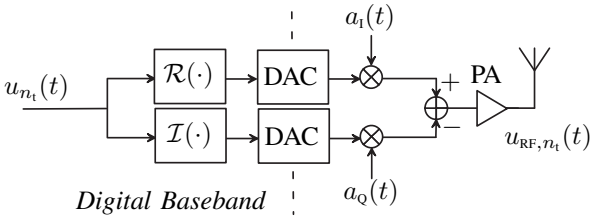

(a) TX front-end

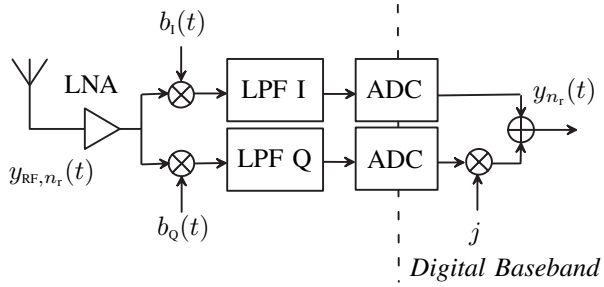

(b) RX front-end

Figure 2. Schematically depicted diagram of the homodyne transceiver.

In the case of perfect matching between the I and Q branch, the local oscillator (LO) signal multiplying the Q signal $a_{\mathrm{Q}}(t)$ is the 90° phase shifted version of the LO signal multiplying the I signal $a_{\mathrm{I}}(t)$. They can, consequently, be expressed as $a_{\mathrm{Q}}(t) = \sin(\omega_{\mathrm{c}} t)$ and $a_{\mathrm{I}}(t) = \cos(\omega_{\mathrm{c}} t)$, where $\omega_{\mathrm{c}} = 2\pi f_{\mathrm{c}}$. Using these expressions, the RF TX signal for the n_{t}th branch can be expressed as

$$\begin{aligned} u_{\mathrm{RF},n_{\mathrm{t}}}(t) &= 2\left(\mathcal{R}\{u_{n_{\mathrm{t}}}(t)\}a_{\mathrm{I}}(t) - \mathcal{I}\{u_{n_{\mathrm{t}}}(t)\}a_{\mathrm{Q}}(t)\right) \\ &= 2\left(\mathcal{R}\{u_{n_{\mathrm{t}}}(t)\}\cos(\omega_{\mathrm{c}} t) - \mathcal{I}\{u_{n_{\mathrm{t}}}(t)\}\sin(\omega_{\mathrm{c}} t)\right) \\ &= u_{n_{\mathrm{t}}}(t)e^{j\omega_{\mathrm{c}} t} + u^*_{n_{\mathrm{t}}}(t)e^{-j\omega_{\mathrm{c}} t}, \end{aligned} \tag{6}$$

where $\mathcal{R}\{\cdot\}$ and $\mathcal{I}\{\cdot\}$ give the real and imaginary part of their arguments and where * denotes complex conjugation. The factor 2 is added for notational convenience.

At the n_{r}th RX branch, as illustrated in Fig. 2(b), the received RF signal $y_{\mathrm{RF},n_{\mathrm{r}}}(t)$ is first amplified by a low-noise amplifier (LNA), which we will, in the analyses of this paper, assume to be perfect with unity gain. Quadrature down-mixing is done again by two 90° phase shifted LO signals at frequency f_{c}. Low-pass filtering is applied in both branches to remove higher order modulation products. Both signals are then passed through the analogue-to-digital convertors (ADCs) and combined to form the baseband signal $y_{n_{\mathrm{r}}}(t)$, which is input to the baseband RX modem.

In the case of perfect matching between the I and Q branch, the LO signals multiplying the I and Q signal again differ by a 90° phase shift. They can, consequently, be expressed as $b_{\mathrm{Q}}(t) = -\sin(\omega_{\mathrm{c}} t)$ and $b_{\mathrm{I}}(t) = \cos(\omega_{\mathrm{c}} t)$. From (6) it can be concluded that the received RF signal on the n_{r}th RX branch is given by

$$y_{\mathrm{RF},n_{\mathrm{r}}}(t) = y_{n_{\mathrm{r}}}(t)e^{j\omega_{\mathrm{c}} t} + y^*_{n_{\mathrm{r}}}(t)e^{-j\omega_{\mathrm{c}} t}. \tag{7}$$

Using the expressions for $b_{\mathrm{I}}(t)$, $b_{\mathrm{Q}}(t)$ and (7), the baseband RX signals can be found to be given by

$$y_{n_{\mathrm{r}}}(t) = y_{\mathrm{I},n_{\mathrm{r}}}(t) + j y_{\mathrm{Q},n_{\mathrm{r}}}(t), \tag{8}$$

where, as we define $\mathrm{LPF}\{\cdot\}$ to be the low-pass filtering operation,

$$\begin{aligned} y_{\mathrm{I},n_{\mathrm{r}}}(t) &= \mathrm{LPF}\{b_{\mathrm{I}}(t)y_{\mathrm{RF},n_{\mathrm{r}}}(t)\} \\ &= \mathrm{LPF}\{\cos(\omega_{\mathrm{c}} t)y_{\mathrm{RF},n_{\mathrm{r}}}(t)\} = \mathcal{R}\{y_{n_{\mathrm{r}}}(t)\}, \end{aligned} \tag{9}$$

$$\begin{aligned} y_{\mathrm{Q},n_{\mathrm{r}}}(t) &= \mathrm{LPF}\{b_{\mathrm{Q}}(t)y_{\mathrm{RF},n_{\mathrm{r}}}(t)\} \\ &= \mathrm{LPF}\{-\sin(\omega_{\mathrm{c}} t)y_{\mathrm{RF},n_{\mathrm{r}}}(t)\} = \mathcal{I}\{y_{n_{\mathrm{r}}}(t)\}. \end{aligned} \tag{10}$$

These results show that for a system with perfect matching the baseband signals are perfectly up-converted in the TX and that the image signal centred around $-f_{\mathrm{c}}$ is perfectly rejected in the down-conversion. In any practical system, however, perfect matching between the I and Q branch of the quadrature TX/RX is not possible due to limited accuracy in the implementation of the RF front-end, the influence of which we will study in the next section.

B. Imperfect IQ matching

The imperfect IQ matching will result in a phase and an amplitude mismatch between the I and Q branch. Several stages in the transceiver structure can contribute to the IQ mismatch, e.g., errors in the nominal 90° phase shift between the LO signals used for up- and down-conversion of the I and Q signals and the difference in amplitude transfer of the total I and Q branches.

These imbalances are generally modelled as phase and/or amplitude errors in the LO signal used for up- and down-conversion, which can be verified to be equivalent to modelling these imbalances in the signal path. The imbalances can be modelled either symmetrical or asymmetrical. In the symmetrical method, each branch (I and Q) experiences half of the phase and amplitude errors, see e.g. [16], [17]. In the asymmetrical method, the I branch is modelled to be ideal and the errors are modelled in the Q branch, see e.g. [9], [18]. It can be verified that these two methods are equivalent. We will use the asymmetrical model for the further analyses in this paper.

For this model the imbalanced LO signals used for up-conversion are given by

$$a_{\mathrm{Q}}(t) = g_{\mathrm{T}} \sin(\omega_{\mathrm{c}} t + \phi_{\mathrm{T}}), \tag{11}$$

$$a_{\mathrm{I}}(t) = \cos(\omega_{\mathrm{c}} t), \tag{12}$$

where g_{T} and ϕ_{T} model the TX gain and phase mismatch, respectively. From the previous section we know that for perfect matching these imbalance parameters are given by $g_{\mathrm{T}} = 1$ and $\phi_{\mathrm{T}} = 0$.

The transmitted RF signal on the n_{t}th branch can then be expressed as

$$\begin{aligned} u_{\mathrm{RF},n_{\mathrm{t}}}(t) &= \left(G_1 u_{n_{\mathrm{t}}}(t) + G_2^* u^*_{n_{\mathrm{t}}}(t)\right) e^{j\omega_{\mathrm{c}} t} \\ &\quad + \left(G_1^* u^*_{n_{\mathrm{t}}}(t) + G_2 u_{n_{\mathrm{t}}}(t)\right) e^{-j\omega_{\mathrm{c}} t}, \end{aligned} \tag{13}$$

where the coefficients G_1 and G_2 are given by

$$G_1 = (1 + g_{\text{T}} e^{j\phi_{\text{T}}})/2, \quad (14)$$
$$G_2 = (1 - g_{\text{T}} e^{-j\phi_{\text{T}}})/2, \quad (15)$$

respectively. It is noted that for perfect TX matching $G_1 = 1$ and $G_2 = 0$ and that (13) reduces to (6).

When we subsequently regard the imbalance in the RX, the imbalanced LO signals used for down-conversion are given by

$$b_{\text{Q}}(t) = -g_{\text{R}} \sin(\omega_{\text{c}} t + \phi_{\text{R}}), \quad (16)$$
$$b_{\text{I}}(t) = \cos(\omega_{\text{c}} t), \quad (17)$$

where g_{R} and ϕ_{R} model the RX gain and phase mismatch, respectively. Note that we can conclude from the previous section that in case of perfect matching, these imbalance parameters are given by $g_{\text{R}} = 1$ and $\phi_{\text{R}} = 0$.

Down-conversion of the RF RX signal, as expressed by (7), then yields

$$\begin{aligned} \hat{y}_{n_{\text{r}}}(t) &= \hat{y}_{\text{I},n_{\text{r}}}(t) + j\hat{y}_{\text{Q},n_{\text{r}}}(t) \\ &= K_1 y_{n_{\text{r}}}(t) + K_2 y^*_{n_{\text{r}}}(t), \end{aligned} \quad (18)$$

where the coefficients K_1 and K_2 are given by

$$K_1 = (1 + g_{\text{R}} e^{-j\phi_{\text{R}}})/2, \quad (19)$$
$$K_2 = (1 - g_{\text{R}} e^{j\phi_{\text{R}}})/2, \quad (20)$$

respectively. Again, for perfect matching we find that $K_1 = 1$ and $K_2 = 0$ and that (18) reduces to (8).

IV. Influence of IQ mismatch on the MIMO OFDM signal model

Now that we have defined a model for the imbalance and have derived its influence on the up- and down-conversion, we will study the influence of IQ mismatch on the detected symbols in a multiple-antenna OFDM system.

We recall that $\mathbf{u}_m$, as defined in (1), denotes the $N_{\text{t}}N_{\text{s}}\times 1$ TX baseband for the mth MIMO OFDM symbol. When this signal is up-converted to RF in the imbalanced quadrature TX, then we find, using (13), that the $N_{\text{t}}\times 1$ vector RF TX vector is given by

$$\begin{aligned} \mathbf{u}_{\text{RF},m}(t) = &\left(\mathbf{G}_1 \mathbf{u}(t) + \mathbf{G}_2^* \mathbf{u}^*(t)\right) e^{j\omega_{\text{c}} t} \\ &+ \left(\mathbf{G}_1^* \mathbf{u}^*(t) + \mathbf{G}_2 \mathbf{u}(t)\right) e^{-j\omega_{\text{c}} t}, \end{aligned} \quad (21)$$

for $t \in \{(m-1)N_{\text{s}}T_{\text{s}}, \ldots, (mN_{\text{s}} - 1)T_{\text{s}}\}$, where $\mathbf{u}((m-1)N_{\text{s}} + n)T_{\text{s}}) = \mathbf{u}_m(n)$ and where T_{s} denotes the sampling time. The diagonal imbalance matrices in (21) are defined by

$$\mathbf{G}_1 = (\mathbf{I} + \boldsymbol{g}_{\text{T}} e^{j\boldsymbol{\phi}_{\text{T}}})/2, \quad (22)$$
$$\mathbf{G}_2 = \mathbf{I} - \mathbf{G}_1^* = (\mathbf{I} - \boldsymbol{g}_{\text{T}} e^{-j\boldsymbol{\phi}_{\text{T}}})/2, \quad (23)$$

where $\mathbf{I}$ denotes the identity matrix and where

$$\boldsymbol{\phi}_{\text{T}} = \text{diag}\{\phi_{\text{T},1}, \phi_{\text{T},2}, \ldots, \phi_{\text{T},N_{\text{t}}}\}, \quad (24)$$
$$\boldsymbol{g}_{\text{T}} = \text{diag}\{g_{\text{T},1}, g_{\text{T},2}, \ldots, g_{\text{T},N_{\text{t}}}\}. \quad (25)$$

We note that (22) and (23) contain different imbalance values for the different TX streams, since it is likely that the different TX branches will exhibit unequal mismatches.

After down-conversion with the imbalanced quadrature RX, the received baseband signal is given by

$$\hat{\mathbf{y}}(t) = \mathbf{K}_1 \mathbf{y}(t) + \mathbf{K}_2 \mathbf{y}^*(t). \quad (26)$$

The diagonal imbalance matrices in (26) are given by

$$\mathbf{K}_1 = (\mathbf{I} + \boldsymbol{g}_{\text{R}} e^{-j\boldsymbol{\phi}_{\text{R}}})/2, \quad (27)$$
$$\mathbf{K}_2 = \mathbf{I} - \mathbf{K}_1^* = (\mathbf{I} - \boldsymbol{g}_{\text{R}} e^{j\boldsymbol{\phi}_{\text{R}}})/2, \quad (28)$$

where

$$\boldsymbol{\phi}_{\text{R}} = \text{diag}\{\phi_{\text{R},1}, \phi_{\text{R},2}, \ldots, \phi_{\text{R},N_{\text{r}}}\}, \quad (29)$$
$$\boldsymbol{g}_{\text{R}} = \text{diag}\{g_{\text{R},1}, g_{\text{R},2}, \ldots, g_{\text{R},N_{\text{r}}}\}. \quad (30)$$

Using the $N_{\text{r}}N_{\text{c}}\times 1$ received frequency-domain vector, as defined in (2), and (4) and (26), we can rewrite the expression for the kth subcarrier as

$$\begin{aligned} \hat{\mathbf{x}}_{m,k} &= \sum_{n=0}^{N_{\text{c}}-1} \hat{\mathbf{y}}_m (N_{\text{g}} + n) e^{-j\frac{2\pi nk}{N_{\text{c}}}} \\ &= \mathbf{K}_1 \mathbf{H}_k \sum_{n=0}^{N_{\text{c}}-1} \hat{\mathbf{u}}_m (N_{\text{g}} + n) e^{-j\frac{2\pi nk}{N_{\text{c}}}} \\ &\quad + \mathbf{K}_2 \mathbf{H}_{-k}^* \sum_{n=0}^{N_{\text{c}}-1} \hat{\mathbf{u}}_m^* (N_{\text{g}} + n) e^{j\frac{2\pi nk}{N_{\text{c}}}}, \end{aligned} \quad (31)$$

where we omitted the noise terms for now for clarity and where the ideal down-converted version of $\mathbf{u}_{\text{RF},m}$ is given by

$$\hat{\mathbf{u}}(t) = \mathbf{G}_1 \mathbf{u}(t) + \mathbf{G}_2^* \mathbf{u}^*(t). \quad (32)$$

Using (1), (21) and (32), we can rewrite (31) as

$$\begin{aligned} \hat{\mathbf{x}}_{m,k} = &\left\{\mathbf{K}_1 \mathbf{H}_k \mathbf{G}_1 + \mathbf{K}_2 \mathbf{H}_{-k}^* \mathbf{G}_2\right\} \mathbf{s}_{m,k} \\ &+ \left\{\mathbf{K}_2 \mathbf{H}_{-k}^* \mathbf{G}_1^* + \mathbf{K}_1 \mathbf{H}_k \mathbf{G}_2^*\right\} \mathbf{s}_{m,-k}^*, \end{aligned} \quad (33)$$

for $k \in \{-K, \ldots, -1, 1, \ldots, K\}$, since we will not regard the DC-carrier, i.e., $k = 0$, since that will not carry data in practical systems due to DC-offset problems.

It can be concluded from (33) that the received frequency-domain vector during the mth symbol on the kth subcarrier is given by the TX vector on that subcarrier, i.e., $\mathbf{s}_{m,k}$, times a complex matrix plus the complex conjugate of the TX vector on the $-k$th carrier, i.e., $\mathbf{s}_{m,-k}^*$, times another complex matrix. The latter component is often referred to as the *mirror signal*, since the subcarrier is located at the same distance from, but at the other side of, the DC-carrier.

When there is perfect TX matching then $\mathbf{G}_1 = \mathbf{I}$ and $\mathbf{G}_2 = \mathbf{0}$ and when there is no RX mismatch then $\mathbf{K}_1 = \mathbf{I}$ and $\mathbf{K}_2 = \mathbf{0}$. Hence, when there is perfect TX and RX matching, (33) reduces to $\mathbf{H}_k \mathbf{s}_{m,k}$, which is the MIMO channel matrix times the transmitted symbol vector.

The influence of IQ imbalance in a system experiencing a frequency-selective channel is shown schematically in Fig. 3, where we assume ideal up-conversion. The transmitted baseband signal is shown in Fig. 3(a), where two subcarriers ($-k$ and k) are highlighted. These subcarriers have the same separation from DC. The signal is

(ideally) up-converted to RF and transmitted through the frequency-selective channel, resulting in the received RF signal depicted in Fig. 3(b). It is clear that subcarrier $-k$ is more attenuated by the channel than subcarrier k. Subsequently, the RX signal is down-converted to baseband using the homodyne structure of Fig. 2(b). Since this structure exhibits IQ mismatch, the mirror signal is not fully rejected, and mixes down into the regarded baseband channel. This is illustrated in Fig. 3(c), which shows that subcarrier k experiences a contribution of the signal received on the mirror subcarrier $-k$ and vice versa. We note that the same behaviour can be observed for a system experiencing a flat-fading channel, however, it that case the magnitudes of the desired signals and leakage contributions are not frequency dependent.

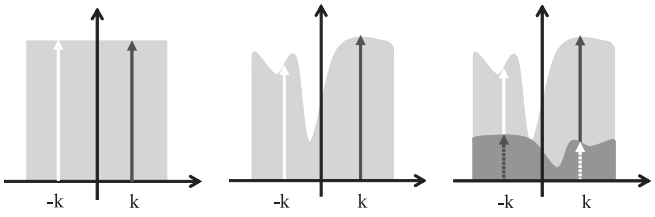

(a) TX baseband (b) RX RF (c) RX baseband

Figure 3. The influence of RX IQ imbalance on the reception of an OFDM signal [11].

To show the effect of the IQ imbalance on the reception of an OFDM signal more clearly, a noiseless single-input single-output (SISO) system applying 16-QAM modulation is regarded. The system does not experience a multipath channel and has a 10% amplitude and 5° phase imbalance between the I and Q branches of the RX. The received signal is depicted in Fig. 4, which shows that the transmitted 16-QAM points are distorted by an additive rotated 16-QAM constellation of lower amplitude. This is due to the leakage of the mirror carrier $-k$, where the rotation and reduced amplitude are due to the imbalance parameter K_2. Furthermore, one can observe a small rotation and a small decrease in amplitude due to the multiplication of the desired signal (on carrier k) with imbalance parameter K_1.

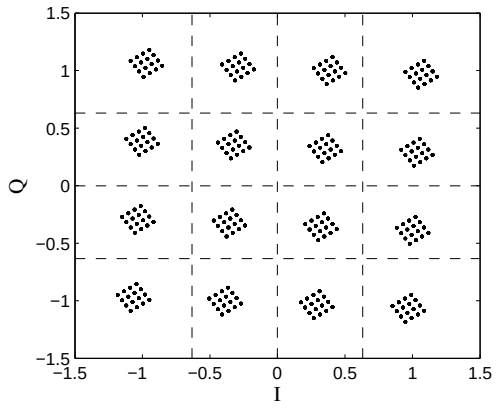

Figure 4. Influence of IQ imbalance on the noiseless reception of 16-QAM symbols.

V. Impact of IQ imbalance on symbol detection

In the previous section, the influence of TX and RX IQ imbalance on the received signal vector in a multiple-antenna OFDM system was investigated. Here this is extended to show the influence on the detection of the transmitted symbols. For that purpose this section studies the error in coherent detection of the transmitted MIMO vector using ZF MIMO detection.

In the foregoing the additive RX noise was omitted to simplify notation. Any practical system will, however, experience this noise term, which changes the expression for the kth carrier of the mth received symbol in (33) to

$$\begin{aligned}\mathbf{x}_{m,k} \;=\; &\big(\mathbf{K}_1\mathbf{H}_k\mathbf{G}_1 + \mathbf{K}_2\mathbf{H}^*_{-k}\mathbf{G}_2\big)\mathbf{s}_{m,k} + \mathbf{K}_1\mathbf{n}_{m,k} \\ &+\big(\mathbf{K}_2\mathbf{H}^*_{-k}\mathbf{G}^*_1 + \mathbf{K}_1\mathbf{H}_k\mathbf{G}^*_2\big)\mathbf{s}^*_{m,-k} + \mathbf{K}_2\mathbf{n}^*_{m,-k}, \end{aligned} \quad (34)$$

where $\mathbf{n}_{m,k}$ denotes the $N_\mathrm{r}\times 1$ additive noise vector for the kth subcarrier during the mth symbol. Note that the noise term is also influenced by the IQ imbalance, since its major source, i.e., the LNA, will be located in front of the down-mixing in any conventional architecture.

When we assume perfect channel knowledge at the RX, the channel estimate is given by the transfer from the TX baseband signals to the RX baseband signals and can be written as

$$\tilde{\mathbf{H}}_k = \mathbf{K}_1\mathbf{H}_k\mathbf{G}_1 + \mathbf{K}_2\mathbf{H}^*_{-k}\mathbf{G}_2, \quad (35)$$

where it is noted that the channel estimate now includes the influence of the TX and RX IQ imbalance. When this transfer is used for ZF-based MIMO processing, the $N_\mathrm{t}\times 1$ estimated TX signal vector for the kth subcarrier is found by (5). It can be verified that the error term is now given by

$$\begin{aligned}\boldsymbol{\varepsilon}_{m,k} \;=\; &\tilde{\mathbf{H}}^\dagger_k\big(\mathbf{K}_2\mathbf{H}^*_{-k}\mathbf{G}^*_1 + \mathbf{K}_1\mathbf{H}_k\mathbf{G}^*_2\big)\mathbf{s}^*_{m,-k} \\ &+\tilde{\mathbf{H}}^\dagger_k\big(\mathbf{K}_1\mathbf{n}_{m,k} + \mathbf{K}_2\mathbf{n}^*_{m,-k}\big). \end{aligned} \quad (36)$$

We can conclude from (36) that the error term includes contributions of the signal term on the mirror carrier $-k$ and of the noise terms corresponding to subcarrier k and $-k$.

When we study the influence of TX and RX IQ imbalance, separately, we find that for a system only experiencing TX or RX IQ imbalance, the error term in (36) is given by

$$\boldsymbol{\varepsilon}_{\mathrm{T},k} = \mathbf{G}_\mathrm{e}\mathbf{s}^*_{m,-k} + \left(\mathbf{H}_k\mathbf{G}_1\right)^\dagger \mathbf{n}_{m,k}, \quad (37)$$

$$\boldsymbol{\varepsilon}_{\mathrm{R},k} = \mathbf{H}^\dagger_k\mathbf{K}_\mathrm{e}\mathbf{H}^*_{-k}\mathbf{s}^*_{m,-k} + \mathbf{H}^\dagger_k\left(\mathbf{K}_\mathrm{e}\mathbf{n}^*_{m,-k} + \mathbf{n}_{m,k}\right), \quad (38)$$

respectively. Here $\mathbf{G}_\mathrm{e}$ and $\mathbf{K}_\mathrm{e}$ are diagonal matrices, defined as $\mathbf{G}_\mathrm{e} = \mathbf{G}^\dagger_1\mathbf{G}^*_2$ and $\mathbf{K}_\mathrm{e} = \mathbf{K}^\dagger_1\mathbf{K}_2$.

When comparing the error term due to TX IQ imbalance in (37) to that of RX IQ imbalance in (38), we conclude that the influence of noise in the error term is almost equal, although $\boldsymbol{\varepsilon}_{\mathrm{R},k}$ also exhibits a small noise contribution from the mirror. Considering the influence of the mirror leakage we can see that the term $\mathbf{G}_\mathrm{e}\mathbf{s}^*_{m,-k}$ in $\boldsymbol{\varepsilon}_{\mathrm{T},k}$ will be of finite size for given $\mathbf{G}_\mathrm{e}$, but that $\mathbf{H}^\dagger_k\mathbf{K}_\mathrm{e}\mathbf{H}^*_{-k}\mathbf{s}^*_{m,-k}$ in $\boldsymbol{\varepsilon}_{\mathrm{R},k}$ can become infinite large for

given $\mathbf{K}_{\mathrm{e}}$, since it contains the multiplication of the channel matrix for carrier $-k$ with the inverse channel matrix for carrier k. When, through fading, the elements of $\mathbf{H}_{-k}$ are large and the elements in $\mathbf{H}_k$ are small, the error term will become large. Since errors in detection are caused by the tails of the error distribution, we can conclude qualitatively that in faded channels the influence of RX IQ imbalance will be larger than that of a comparable TX IQ imbalance.

VI. Probability of erroneous detection for M-QAM modulation

Although the previous section provides a qualitative distinction between the influence of TX and RX IQ imbalance, a quantitative study is required to provide a more precise understanding of the impact on system performance. For that purpose we will, in this section, study the influence of the error vector $\boldsymbol{\varepsilon}_{m,k}$ in (36) on the detection of the transmitted vector $\mathbf{s}_{m,k}$. We will calculate the probability of erroneous detection of transmit signals chosen from a rectangular M-QAM constellation. The influence is derived, separately, for TX and RX IQ imbalance in Sections VI-A and VI-B, respectively.

A. TX IQ imbalance

Let us first consider the case of TX IQ imbalance, where the error term $\boldsymbol{\varepsilon}_{\mathrm{T}}$ is defined by (37). In our approach to calculate the probability of error, we will first consider leakage from the mirror subcarrier as a translation of the wanted signal term. Later on, we will average over all possible realisations of the mirror signal.

When we assume that the estimated signal on carrier k in symbol m is translated by the known $N_{\mathrm{t}}\times 1$ vector

$$\mathbf{d}_{m,k} = \mathbf{G}_{\mathrm{e}}\mathbf{s}^{*}_{m,-k}, \tag{39}$$

the error in the estimated translated TX signal is found by combining (37) and (39), yielding

$$\boldsymbol{\varepsilon}'_{\mathrm{T},k} = \boldsymbol{\varepsilon}_{\mathrm{T},k} - \mathbf{d}_{m,k} = \left(\mathbf{H}_k\mathbf{G}_1\right)^{\dagger}\mathbf{n}_{m,k} = \mathbf{H}_k^{\dagger}\mathbf{n}'_{m,k}. \tag{40}$$

Here $\mathbf{n}'_{m,k} \sim \mathcal{CN}(\mathbf{0}, (\sigma_n^2/|G_1|^2)\mathbf{I})$ and we assumed the IQ imbalance to be equal on all TX branches, i.e., $\mathbf{G}_1 = G_1\mathbf{I}$. We note that it can be verified that the real and imaginary part of the elements of $\mathbf{n}'_{m,k}$ are i.i.d., since the elements of $\mathbf{n}_{m,k}$ are i.i.d. Note also that

$$\boldsymbol{\mu}_{\mathrm{T}} = \mathbb{E}\left[\boldsymbol{\varepsilon}'_{\mathrm{T},k}\right] = \mathbf{0}, \tag{41}$$

since the mean of the elements of $\mathbf{n}_{m,k}$ equals zero, and that the covariance matrix of the error in (40) is given by

$$\boldsymbol{\Omega}_{\mathrm{T}} = \mathbb{E}\left[\boldsymbol{\varepsilon}'_{\mathrm{T},k}\{\boldsymbol{\varepsilon}'_{\mathrm{T},k}\}^{H}\middle|\mathbf{G}_1, \mathbf{H}_k\right] = \frac{\sigma_{\mathrm{n}}^2}{|G_1|^2}\left(\mathbf{H}_k^H\mathbf{H}_k\right)^{-1}, \tag{42}$$

where $\mathbb{E}\left[\mathbf{X}\middle|\mathbf{Y}\right]$ denotes the conditional expected value of $\mathbf{X}$ given $\mathbf{Y}$.

The effective SNR for the n_{t}th branch and kth carrier can, subsequently, be found using (42) and is given by

$$\wp_{n_{\mathrm{t}},k} = \frac{|G_1|^2\sigma_{\mathrm{s}}^2}{\sigma_{\mathrm{n}}^2\left[\left(\mathbf{H}_k^H\mathbf{H}_k\right)^{-1}\right]_{n_{\mathrm{t}}n_{\mathrm{t}}}}, \tag{43}$$

where $[\mathbf{A}]_{mm}$ denotes the mth diagonal element of the matrix $\mathbf{A}$ and the covariance matrix of $\mathbf{s}_m$ equals $\sigma_{\mathrm{s}}^2\mathbf{I}$. When the channel matrix $\mathbf{H}_k$ has i.i.d. complex Gaussian entries, often referred to as Rayleigh fading, $\wp_{n_{\mathrm{t}},k}$ is chi-square distributed with $2R = 2(N_{\mathrm{r}} - N_{\mathrm{t}} + 1)$ degrees of freedom. The pdf of $\wp_{n_{\mathrm{t}}}(k)$ is then given by

$$p_{\wp_{n_{\mathrm{t}},k}}(\rho) = \frac{(\rho/\wp_0)^{R-1}}{\wp_0(R-1)!}\exp(-\rho/\wp_0), \tag{44}$$

where $\wp_0$ is the average SNR, given by

$$\wp_0 = |G_1|^2\sigma_{\mathrm{s}}^2/\sigma_{\mathrm{n}}^2. \tag{45}$$

Now we have found the distribution of the SNR, we can proceed to the second step of the derivation, in which we derive the probability of erroneous detection for a given SNR.

In the remainder, we will consider one carrier in one of the TX streams and, therefore, omit the subcarrier and branch index, i.e., we abbreviate $\wp_{n_{\mathrm{t}},k} = \wp$. Since the statistics are equal for all subcarriers and TX streams, the resulting probability of error can easily be generalised for all carriers later on.

If we first consider the probability of erroneous detection of rectangular M-QAM symbols for a given SNR $\wp$ and a given translation $d = d_{\mathrm{R}} + jd_{\mathrm{I}}$, we can use the independence of the real and imaginary part of the estimated symbols. Consequently, the probability of erroneous detection of rectangular M-QAM symbols can be derived by using two $\sqrt{M}$-dimensional pulse-amplitude-modulation ($\sqrt{M}$-PAM) signals, one for the real and one for the imaginary part. The probability of symbol error is then given by

$$P^{d}_{\mathrm{e},M\text{-QAM},E_{\mathrm{s}}} = 1 - (1 - P^{d_{\mathrm{R}}}_{\mathrm{e},\sqrt{M}\text{-PAM},E_{\mathrm{s}}/2})(1 - P^{d_{\mathrm{I}}}_{\mathrm{e},\sqrt{M}\text{-PAM},E_{\mathrm{s}}/2}), \tag{46}$$

where $P^{d_{\mathrm{R}}}_{\mathrm{e},\sqrt{M}\text{-PAM},E_{\mathrm{s}}/2}$ and $P^{d_{\mathrm{I}}}_{\mathrm{e},\sqrt{M}\text{-PAM},E_{\mathrm{s}}/2}$ denote the probability of error for the d-translated $\sqrt{M}$-PAM modulation for the real and imaginary part of the M-QAM constellation, respectively. The power of these PAM signals is half of that of the QAM symbols. We recall that the translation due to TX IQ imbalance was defined in (39).

The influence of a translation of d_{R} on the 4-PAM constellation is schematically depicted in Fig. 5.

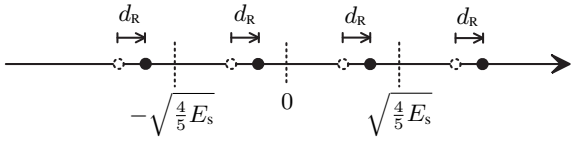

Figure 5. Influence of d_{R}-translation on the 4-PAM constellation.

The original 4-PAM constellation points are depicted by dashed white dots, the translated symbols are depicted by black dots and the *decision boundaries* are depicted by dashed lines. For the original constellation point, the distances to the decision boundaries are $\sqrt{E_{\mathrm{s}}/5}$, i.e., when the absolute value of the error in symbol estimation is larger than $\sqrt{E_{\mathrm{s}}/5}$ a symbol error occurs. It is clear from the figure that the distances to the decision boundaries

are changed from the original $\sqrt{E_s/5}$ for the translated symbols. For half of the cases the distances now equals $\sqrt{E_s/5}-d_R$ and the other half $\sqrt{E_s/5}+d_R$, where the smallest one will impose the highest error probability.

When we now generalise the observations from Fig. 5, we find that for the real part the probability of error of an $\sqrt{M}$-PAM system is given by

$$P^{d_R}_{e,\sqrt{M}\text{-PAM},E_s} = \frac{a_1}{2}\left(\mathbb{P}\left(|\varepsilon'|>a_2-d_R\right)+\mathbb{P}\left(|\varepsilon'|>a_2+d_R\right)\right) = a_1\left(Q\left(\frac{a_2-d_R}{\sqrt{N_0/2}}\right)+Q\left(\frac{a_2+d_R}{\sqrt{N_0/2}}\right)\right), \quad (47)$$

where $a_1=1-1/\sqrt{M}$, $a_2=\sqrt{\frac{3E_s}{M-1}}$, $d_R=\mathcal{R}\{G_e s^*_{-k}\}$, $Q(x)$ denotes the Q-function or complementary cumulative normal distribution function and where N_0 denotes the noise power spectral density. A similar derivation for $P^{d_I}_{e,\sqrt{M}\text{-PAM},E_s}$ yields the same results as (47), where d_R is replaced with $d_I=\mathcal{I}\{G_e s^*_{-k}\}$. Substituting this into (46) yields

$$P^{d}_{e,M\text{-QAM}} = 1-\left(1-c_1\left(\mathcal{U}(c_2\wp,\sqrt{2}d_R)+\mathcal{U}(c_2\wp,-\sqrt{2}d_R)\right)\right) \cdot\left(1-c_1\left(\mathcal{U}(c_2\wp,\sqrt{2}d_I)+\mathcal{U}(c_2\wp,-\sqrt{2}d_I)\right)\right), \quad (48)$$

where $\mathcal{U}(a,b)=Q\left(\sqrt{a}-\frac{b}{\sqrt{N_0}}\right)$, $c_1=1-1/\sqrt{M}$, $c_2=3/(M-1)$ and the SNR is defined as $\wp=E_s/N_0$. For high SNR-values, (48) is well approximated by

$$P^{d}_{e,M\text{-QAM}} \approx c_1\left(\mathcal{U}(c_2\wp,-\sqrt{2}|d_R|)+\mathcal{U}(c_2\wp,-\sqrt{2}|d_I|)\right). \quad (49)$$

We note that (48) was calculated for a given s_{-k}, but that we aim at the averaged SER over all possible realisations of s_{-k}. Since the d values originate from the M-QAM constellation, the probability of the occurrence of the different symbols has a discrete uniform distribution. The average probability of error is thus given by

$$P^{av}_{e,M\text{-QAM}} = \frac{1}{M}\sum_{q=1}^{M} P^{d_q}_{e,M\text{-QAM}}, \quad (50)$$

where d_q is the mirror interference term, which is a multiplication of the (given) G_e and the qth symbol out of the M-QAM modulation alphabet.

When we, as an example, work out the above for 4-QAM modulation, we find that the possible values of the translation are given by

$$d_q = G_e\frac{\sqrt{E_s}(\pm1\pm j)}{\sqrt{2}} = \frac{1-g_T e^{j\phi_T}}{1+g_T e^{j\phi_T}}\frac{\sqrt{E_s}(\pm1\pm j)}{\sqrt{2}}, \quad (51)$$

all with equal probability. It is then verified that due to symmetry $P^{d_q}_{e,M\text{-QAM}}$ is equal for all $q\in\{1,\ldots,4\}$ and that the average probability of error in (50) is given by

$$P^{av}_{e,4\text{-QAM}} = \frac{\mathcal{V}(\wp,g_S)+\mathcal{V}(\wp,-g_S)+\mathcal{V}(\wp,g_D)+\mathcal{V}(\wp,-g_D)}{2} - \frac{\left[\mathcal{V}(\wp,g_S)+\mathcal{V}(\wp,-g_S)\right]\left[\mathcal{V}(\wp,g_D)+\mathcal{V}(\wp,-g_D)\right]}{4}. \quad (52)$$

Here, we defined $\mathcal{V}(a,b)=Q\left(\sqrt{a}(1-b)\right)$, $g_S=g_R+g_I$, $g_D=g_R-g_I$ and

$$g_R=\mathcal{R}\{G_e\}=(1-g_T^2)/\left(1+g_T^2+2g_T\cos(\phi_T)\right), \quad (53)$$

$$g_I=\mathcal{I}\{G_e\}=-2g_T\sin(\phi_T)/\left(1+g_T^2+2g_T\cos(\phi_T)\right). \quad (54)$$

The SER expression in (52) can be approximated for the high SNR region by

$$P^{av}_{e,4\text{-QAM}} \approx \frac{1}{2}\left[Q\left(\sqrt{\wp}(1-g_S)\right)+Q\left(\sqrt{\wp}(1-g_D)\right) +Q\left(\sqrt{\wp}(1+g_S)\right)+Q\left(\sqrt{\wp}(1+g_D)\right)\right]. \quad (55)$$

It can be concluded from (55) and Fig. 5 that the TX IQ imbalance will result in a shifting of the SER curves. Flooring in the SER performance will, however, only occur for IQ imbalance values where the translated constellation point are located outside the correct decision region, i.e., when the factor multiplying $\sqrt{\wp}$ is smaller than or equal to 0. For even higher SNR values the last two terms in (55) can also be omitted.

The expressions in (52) and (55) provide the SER for a system experiencing TX IQ imbalance, but *no* fading channel, i.e., for a given SNR $\wp$. To calculate the average SER for faded channels, we have to integrate these SER expressions over the distribution of the SNR in (44). The SER for the n_tth branch and kth subcarrier of an uncoded system is then found by

$$P_e = \int_0^\infty P^{av}_{e,M\text{-QAM}}(\rho)p_\wp(\rho)d\rho, \quad (56)$$

where the subcarrier and branch index were omitted for readability. The final expression for a MIMO OFDM system experiencing TX IQ imbalance and an i.i.d. Rayleigh faded channel is then found by substituting (44) and (50) into (56) and then averaging over all subcarriers and TX branches. A closed form SER expression can be found using a similar approach as we will use for RX IQ imbalance in Section VI-B, yielding an expression based on hypergeometric functions.

For the 4-QAM example, the SER for a fading channel can be found by substituting (44) and either (55) or (52) into (56). The final average SER expression is then found by averaging over all carriers and TX branches.

B. RX IQ imbalance

Let us, subsequently, consider the case of RX IQ imbalance for which the error vector $\boldsymbol{\varepsilon}_R$ is given by (38). The mean of this error term is given by

$$\boldsymbol{\mu}_R = \mathbb{E}\left[\boldsymbol{\varepsilon}_{R,k}\right]=\mathbf{0}, \quad (57)$$

since the elements of $\mathbf{s}^*_{m,-k}$ and $\mathbf{n}_{m,k}$ have zero mean.

The covariance matrix of the error vector for the kth carrier is given by

$$\begin{aligned}\boldsymbol{\Omega}_R &= \mathbb{E}\left[\boldsymbol{\varepsilon}_{R,k}\boldsymbol{\varepsilon}^H_{R,k}\middle|\mathbf{K}_e,\mathbf{H}(k)\right]\\ &= \mathbb{E}\left[\mathbf{H}^\dagger_k\mathbf{K}_e\mathbf{H}^*_{-k}\mathbf{s}^*_{m,-k}\mathbf{s}^T_{m,-k}\mathbf{H}^T_{-k}\mathbf{K}^H_e\{\mathbf{H}^\dagger_k\}^H\right]\\ &\quad+\mathbb{E}\left[\mathbf{H}^\dagger_k\mathbf{K}_e\mathbf{n}^*_{m,-k}\mathbf{n}^T_{m,-k}\mathbf{K}^H_e\{\mathbf{H}^\dagger_k\}^H\right]\\ &\quad+\mathbb{E}\left[\mathbf{H}^\dagger_k\mathbf{n}_{m,k}\mathbf{n}^H_{m,k}\{\mathbf{H}^\dagger_k\}^H\right]\\ &= (N_t\sigma_s^2+\sigma_n^2)\mathbf{H}^\dagger_k\mathbf{K}_e\mathbf{K}^H_e\{\mathbf{H}^\dagger_k\}^H+\sigma_n^2\left(\mathbf{H}^H_k\mathbf{H}_k\right)^{-1}\\ &= \left(|K_e|^2N_t\sigma_s^2+(1+|K_e|^2)\sigma_n^2\right)\left(\mathbf{H}^H_k\mathbf{H}_k\right)^{-1}, \quad (58)\end{aligned}$$

where we assumed $\mathbf{H}_{-k}$ to be independent of $\mathbf{H}_k$, which was shown in [11] to be a reasonable assumption for a practical system experiencing indoor multipath channels. Furthermore, we assumed in (58) that the IQ imbalance on all RX branches was equal, i.e., $\mathbf{K}_\mathrm{e} = K_\mathrm{e}\mathbf{I}$. The effective SNR for the n_tth branch and the kth carrier, is then found from (58) and given by

$$\wp_{n_\mathrm{t},k} = \frac{\sigma_\mathrm{s}^2 \left\{ \left[\left(\mathbf{H}_k^H \mathbf{H}_k \right)^{-1} \right]_{n_\mathrm{t} n_\mathrm{t}} \right\}^{-1}}{|K_\mathrm{e}|^2 N_\mathrm{t} \sigma_\mathrm{s}^2 + (1+|K_\mathrm{e}|^2)\sigma_\mathrm{n}^2}. \quad (59)$$

Note again, that when the channel matrix $\mathbf{H}_k$ has i.i.d. complex Gaussian entries, $\wp_{n_\mathrm{t},k}$ is chi-square distributed with $2R{=}2(N_\mathrm{r} - N_\mathrm{t} + 1)$ degrees of freedom and that its pdf is given by (44). The average SNR is here given by

$$\wp_0 = \frac{\sigma_\mathrm{s}^2}{|K_\mathrm{e}|^2 N_\mathrm{t} \sigma_\mathrm{s}^2 + (1+|K_\mathrm{e}|^2)\sigma_\mathrm{n}^2}. \quad (60)$$

The SER for the n_tth branch and kth subcarrier of an uncoded system is then found using (56), where $P_{\mathrm{e},M\text{-QAM}}^{\mathrm{av}} = P_{\mathrm{e},M\text{-QAM}}$ is the approximation of the SER for an M-QAM constellation and it is given by

$$P_{\mathrm{e},M\text{-QAM}}(\wp) = c_3 Q(\sqrt{c_2 \wp}). \quad (61)$$

In this expression $c_3 = 4(1 - 1/\sqrt{M})$ and we recall that $c_2 = 3/(M-1)$. The average SER is now found by averaging P_e over the different subcarriers and branches. The average (approximate) bit-error rate (BER) is then found by dividing the SER by $\log_2(M)$.

To derive a closed form expression for the SER, we use an alternative representation for the Gaussian Q-function [19, p.71], given by

$$Q(x) = \frac{1}{\pi} \int_0^{\pi/2} \exp\left(-\frac{x^2}{2\sin^2\varphi} \right) d\varphi \quad \text{for} \quad x \geq 0. \quad (62)$$

By substituting this expression and (44) into (56), working out one integral and by change of integration variable, we find that the probability of symbol error is given by

$$\begin{aligned} P_\mathrm{e} &= \frac{c_3}{\pi} \int_0^\infty \int_0^{\pi/2} \exp\left(-\frac{c_2 \wp}{2\sin^2\varphi} \right) d\varphi p_\wp(\rho) d\rho \\ &= \frac{c_3}{\pi} \int_0^{\pi/2} \left(1 + \frac{c_2 \wp_0}{2\sin^2\varphi} \right)^{-R} d\varphi \\ &= \frac{c_3(1 - \sqrt{\wp_0 c_4})}{2} \, {}_2F_1\left(\frac{1}{2}, R + \frac{1}{2}; \frac{3}{2}; \frac{-c_2\wp_0}{2} \right), \end{aligned} \quad (63)$$

where $c_4 = \sqrt{\frac{2c_2}{\pi}} \frac{(R-\frac{1}{2})!}{(R-1)!}$ and ${}_2F_1$ denotes the hypergeometric function [20]. For the special case where the number of TX and RX branches is equal, i.e., $R = 1$, we can use the findings of [21] for AWGN distorted ZF-based MIMO systems, which show that (63) reduces to

$$P_\mathrm{e} = \frac{c_3}{2} \left(1 - \sqrt{\frac{c_2 \wp_0}{2 + c_2 \wp_0}} \right). \quad (64)$$

VII. Numerical results

The analytical results derived in the previous section are here compared with results from Monte Carlo simulations. All simulations are carried out for a MIMO OFDM system based on the IEEE 802.11a standard [22], as described in [4]. For these simulations all 64 subcarriers contain data symbols and no coding is applied. It is assumed that the MIMO transfer is perfectly estimated, yielding the estimate expressed in (35). In the simulated scenarios all TX or RX branches exhibit the same IQ imbalance. All figures presented in this section depict the analytical results by lines and the results from simulations by markers.

First the influence of TX IQ imbalance in an AWGN channel is studied. A SISO system applying 64-QAM modulation experiencing different values of IQ imbalance is simulated. The SER results are reported in Fig. 6 together with the analytical results found using (50). The results are depicted as a function of the average SNR per RX antenna, which is given by $N_\mathrm{t}\sigma_\mathrm{s}^2/\sigma_\mathrm{n}^2$, i.e., $\sigma_\mathrm{s}^2/\sigma_\mathrm{n}^2$ for the regarded SISO system. We note that this definition was chosen to allow for a fair comparison between the different antenna configurations. For a given SNR and noise power, the power per TX branch is scaled by $1/N_\mathrm{t}$, such that the total TX power is independent of the number of TX antennas.

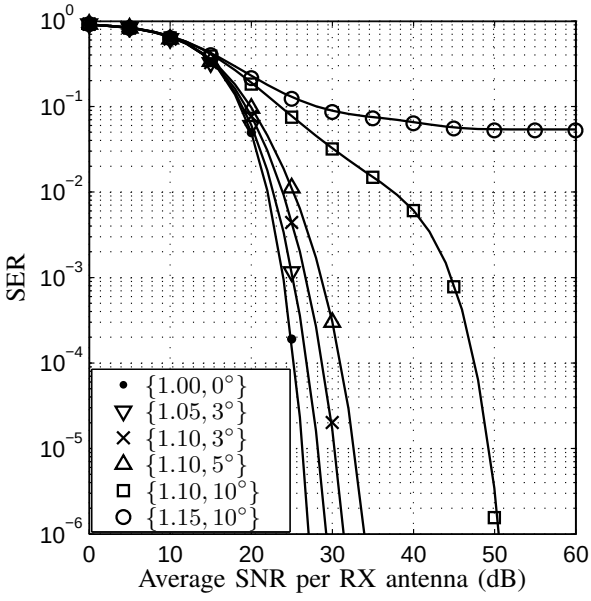

Figure 6. SER performance of a system experiencing TX IQ imbalance and an AWGN channel. Results are depicted for an 1×1 64-QAM system. Analytical results of (50). The figure legend reports the IQ imbalance parameters $\{g_\mathrm{T}, \phi_\mathrm{T}\}$.

It can be concluded from Fig. 6 that the analytical results accurately predict the SER results found from simulations, proving the applicability of the results derived in (50). It can furthermore be concluded that considerable degradation only occurs for very high values of IQ imbalance. Additionally, although degradation in SER performance occurs, flooring of the curves only seems to occur for $g_\mathrm{T} = 1.15$ and $\phi_\mathrm{T} = 10°$, where the translation

d is such that some of the 64-QAM constellation points are shifted outside their decision regions. For these cases, the coefficient multiplying the $\sqrt{\wp}$ in at least one of the Q-functions forming the SER expression is smaller than or equal to 0.

Similar results are depicted in Fig. 7, but now for a system applying a 4-QAM modulation. The results from simulations are compared with the analytical results of (52) and (55), which are the derived exact SER and high SNR approximation of the SER, respectively.

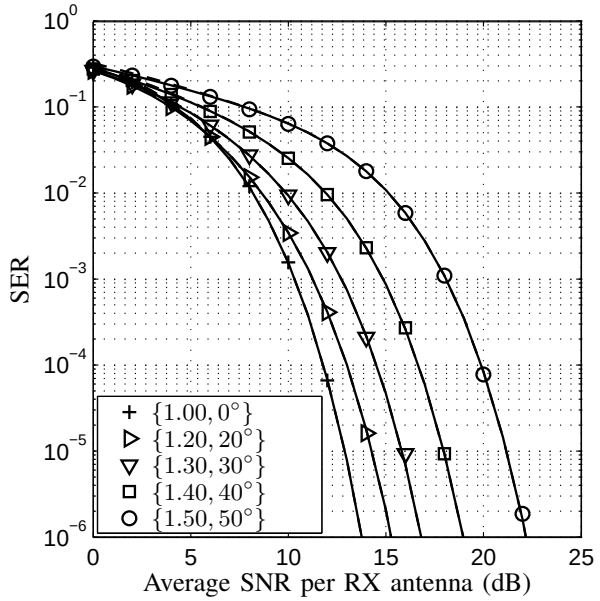

Figure 7. SER performance of a system experiencing TX IQ imbalance and an AWGN channel. Results are depicted for an 1×1 4-QAM system. The exact analytical results of (52) (solid lines) and approximate SER results of (55) (dashed lines) are depicted. The figure legend reports $\{g_{\text{T}}, \phi_{\text{T}}\}$.

The results presented in Fig. 7 allow the conclusion that both the exact as well as the approximate analytical expressions for the SER correctly predict the system performance. A small disparity between the curves is only visible for SNR values below 5 dB. It is furthermore clear from the figure that SER degradation due to TX IQ imbalance only occurs for very high imbalance values and that no flooring occurs for the regarded values of IQ imbalance.

The SER results for different MIMO systems experiencing TX IQ imbalance and a fading channel are depicted in Fig. 8. The figure compares the analytical results of (56) with simulation results for 1×1, 2×2 and 2×4 4-QAM system. In these simulations independent fading over the antennas and subcarriers was simulated. We observe in Fig. 8 that also for the Rayleigh fading channel the analytical expressions accurately predict the error performance. Furthermore, we conclude that the influence of the TX IQ imbalance on the performance of the symmetric MIMO systems is small. At a SER of 10^{-2}, the degradation for these systems is 0.3 dB and 3.8 dB for $g_{\text{T}} = 1.30$, $\phi_{\text{T}} = 30°$ and $g_{\text{T}} = 1.50$, $\phi_{\text{T}} = 50°$, respectively. For the 2×4 system this is 0.9 dB and 6 dB, respectively. We note, however, that in none of the cases

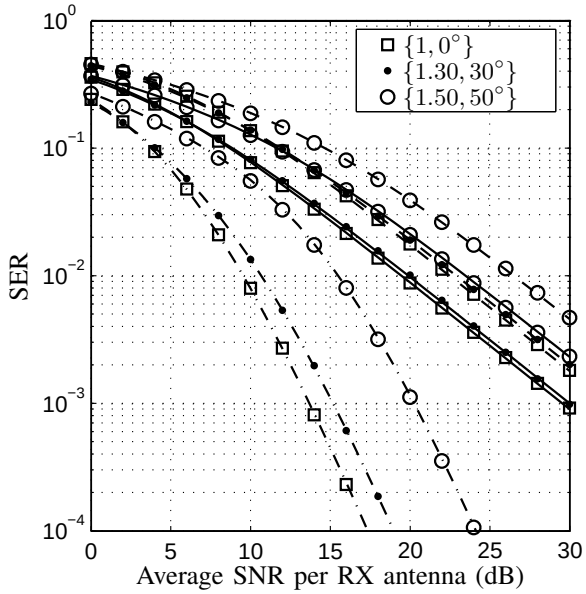

Figure 8. SER performance of a system experiencing TX IQ imbalance and a Rayleigh fading channel. Results are depicted for an 1×1 (solid lines), 2×2 (dashed lines) and 2×4 (dash-dot lines) 4-QAM system. IQ imbalance is equal on TX branches. The figure legend reports $\{g_{\text{T}}, \phi_{\text{T}}\}$.

flooring in the SER performance occurs. Furthermore, although the IQ imbalance of $g_{\text{T}} = 1.30$, $\phi_{\text{T}} = 30°$ is very high, the SER degradation is below 1 dB at a SER of 10^{-2} for all the studied systems.

Results of simulations testing the influence of RX IQ imbalance are depicted in Fig. 9 together with the corresponding analytical results of (63). Results are depicted for an 1×1 and 2×2 64-QAM and a 2×2 4-QAM system.

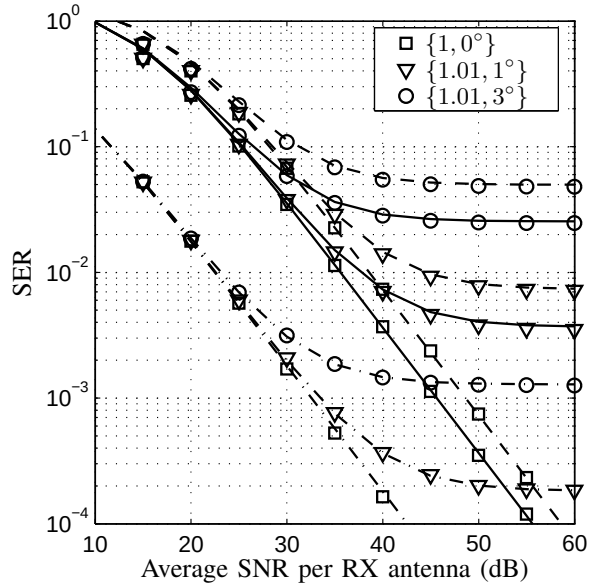

Figure 9. SER performance of systems experiencing RX IQ imbalance and a Rayleigh fading channel. Results are depicted for a 1×1 64-QAM (solid lines), 2×2 64-QAM (dashed lines) and 2×2 4-QAM (dash-dot lines) system. Analytical results of (63) are in lines and simulation results are depicted by markers. The figure legend reports $\{g_{\text{R}}, \phi_{\text{R}}\}$.

We conclude from the results in Fig. 9 that also for RX IQ imbalance in MIMO OFDM systems the analytical SER expressions derived in the previous section are well

applicable. When comparing the results with those in Fig. 8, we conclude that the degradation due to the much lower RX IQ imbalance is considerably higher than that of TX IQ imbalance, as was already qualitatively concluded in Section V. It is noted, furthermore, that these small values of RX IQ imbalance already cause flooring in the SER performance. This in contrast to TX IQ imbalance, where flooring only occurs for very severe mismatch.

VIII. Discussion and Conclusions

The impact of IQ imbalance on the performance of zero-IF based multiple-antenna OFDM systems has been studied in this paper. First, a model for the transceiver structure was introduced, which was used to derive the influence of both TX and RX IQ imbalance on the received signal. It is concluded that IQ imbalance in MIMO OFDM results in scaling and rotation of the signals and in signal leakage from the DC-mirrored subcarrier. The error in the estimation of the TX vector was derived for both TX and RX IQ imbalance, which allowed for the qualitative conclusion that in fading channels the influence of RX IQ imbalance will be greater than that of TX IQ imbalance.

To further substantiate this conclusion, an analytical study of the probability of erroneous detection of transmitted M-QAM symbols was performed. Analytical closed-form expressions for the symbol-error rate (SER) were derived. These results were compared with results from a simulation study, confirming that the derived analytical expressions can be used to accurately predict the SER of a MIMO OFDM system experiencing IQ imbalance for a wide range of imbalance parameters. From these results it can be concluded that in case of fading channels RX IQ imbalance is on average more destructive than TX IQ imbalance. Additionally, it is concluded that the addition of extra RX antennas is beneficial to reduce the dependence on RX IQ imbalance, but increases at the same time the impact of TX IQ imbalance.

The observed differences between the influence of TX and RX IQ imbalance can intuitively be understood as follows. For both cases the IQ imbalance results in leakage of the signal on the mirror subcarrier. For the TX IQ imbalance, the leakage consists of, scaled and rotated, M-QAM symbols, see (37). In detection this can be considered equal to shifting of the decision boundaries. For the RX IQ imbalance, the leakage consists of M-QAM symbols multiplied with the channel matrix, see (38). For a Rayleigh fading channel, the leakage can be approximated as an additional Gaussian RX noise term. As such, the influence is similar to that of the commonly studied additive Gaussian RX noise source, i.e., the SER performance (and thus the SER flooring) depends on the MIMO configuration.

References

[1] T. C. W. Schenk, E. R. Fledderus, and P. F. M. Smulders, "Performance impact of IQ mismatch in direct-conversion MIMO OFDM transceivers," in *Proc. IEEE Radio and Wireless Symposium (RWS 2007), Long Beach (CA)*, Jan. 2007, pp. 329–332.

[2] H. Sampath, S. Talwar, J. Tellado, V. Erceg, and A. Paulraj, "A fourth-generation MIMO-OFDM broadband wireless system: design, performance, and field trial results," *IEEE Commun. Magazine*, vol. 40, no. 9, pp. 143–149, Sept. 2002.

[3] G. L. Stüber, J. Barry, S. W. McLaughlin, Y. Li, M. A. Ingram, and T. G. Pratt, "Broadband MIMO-OFDM wireless communications," *IEEE Proceedings*, vol. 92, no. 2, pp. 271–294, April 2004.

[4] A. v. Zelst and T. C. W. Schenk, "Implementation of a MIMO OFDM-based wireless LAN system," *IEEE Trans. on Sign. Proc.*, vol. 52, no. 2, pp. 483–494, Feb. 2004.

[5] A. A. Abidi, "Direct-conversion radio transceivers for digital communications," *IEEE Journ. of Solid-State Circuits*, vol. 30, pp. 1399–1410, Dec. 1995.

[6] B. Razavi, "Design considerations for direct-conversion receivers," *IEEE Trans. on Circuits and Systems II: Analog and Digital Signal Processing*, vol. 44, no. 6, pp. 428–435, June 1997.

[7] C.-L. Liu, "Impacts of I/Q imbalance on QPSK-OFDM-QAM detection," *IEEE Trans. Consum. Elect.*, vol. 44, no. 3, pp. 984–989, Aug. 1998.

[8] M. Buchholz, A. Schuchert, and R. Hasholzner, "Effects of tuner IQ imbalance on multicarrier-modulation systems," in *Proc. the 2000 3th IEEE ICCDCS*, March 2000, pp. T65/1 – T65/6.

[9] M. Valkama, M. Renfors, and V. Koivunen, "Advanced methods for I/Q imbalance compensation in communication receivers," *IEEE Trans. on Signal Proc.*, vol. 49, pp. 2335–2344, Oct. 2001.

[10] M. Valkama, Y. Zou, and M. Renfors, "On I/Q imbalance effects in MIMO space-time coded transmission systems," in *Proc. IEEE Radio and Wireless Symposium (RWS 2006), San Diego*, Jan. 2006, pp. 223–226.

[11] M. Windisch and G. Fettweis, "Performance degradation due to I/Q imbalance in multi-carrier direct conversion receivers: A theoretical analysis," in *Proc. IEEE Int. Conf. on Commun., Istanbul, Turkey*, vol. 1, June 2006, pp. 257–262.

[12] R. M. Rao and B. Daneshrad, "I/Q mismatch cancellation for MIMO-OFDM systems," in *Proc. IEEE Int. Symp. Pers., Indoor, Mobile Radio Commun. (PIMRC)*, vol. 5, Sept. 2004, pp. 2710–2714.

[13] A. Tarighat and A. H. Sayed, "MIMO OFDM receivers for systems with IQ imbalances," *IEEE Trans. on Sign. Proc.*, vol. 53, no. 9, pp. 3583–3596, Sept. 2005.

[14] T. C. W. Schenk, P. F. M. Smulders, and E. R. Fledderus, "Estimation and compensation of TX and RX IQ imbalance in OFDM based MIMO systems," in *Proc. IEEE Radio and Wireless Symposium (RWS 2006)*, Jan. 2006, pp. 215–218.

[15] T. C. W. Schenk, P. F. M. Smulders, and E. R. Fledderus, "Estimation and compensation of frequency selective TX/RX IQ imbalance in MIMO OFDM systems," in *Proc. IEEE Int. Conf. on Commun., Istanbul, Turkey*, vol. 1, June 2006, pp. 251 – 256.

[16] B. Razavi, *RF Microelectronics*, ser. Prentice-Hall Communications Engineering and Emerging Technologies Series. Prentice Hall, 1998.

[17] J. Tubbax, B. Côme, L. van der Perre, L. Deneire, S. Donnay, and M. Engels, "Compensation of IQ imbalance in OFDM systems," in *Proc. IEEE International Conf. on Commun. 2003*, vol. 5, May 2003, pp. 3403–3407.

[18] M. Windisch and G. Fettweis, "Standard-independent I/Q imbalance compensation in OFDM direct-conversion receivers," in *Proc. 9th International OFDM Workshop*, Sept. 2004, pp. 57–61.

[19] M. K. Simon and M. S. Alouni, *Digital Communication over Fading Channels, A Unified Approach to Performance Analysis*. Wiley, NY, 2000.

[20] N. M. Temme, *Speciale functies in de mathematische fysica*. Epsilon Uitgaven, 1990.
[21] M. Kiessling and J. Speidel, "Analytical performance of MIMO zero-forcing receivers in correlated Rayleigh fading environments," in *Proc. IEEE SPAWC 2003*, June 2003, pp. 383–387.
[22] *IEEE 802.11a standard*. ISO/IEC 802-11:1999/Amd 1:2000(E), Wireless LAN Medium Access Control (MAC) and Physical Layer (PHY) specifications − Amendment 1: High-speed Physical Layer in the 5 GHz band.

Tim C. W. Schenk received the M.Sc. and Ph.D. degrees in electrical engineering from Eindhoven University of Technology (TU/e), Eindhoven, The Netherlands, in 2002 and 2006, respectively. The dissertation topic for his Ph.D. degree concerned the influence and digital compensation of front-end impairments in multiple-antenna multicarrier systems.

From 2002 to 2004, he was with the Wireless Systems Research group at Agere Systems, Nieuwegein, The Netherlands. From 2004 to 2006, he was a Research Assistant in the Radiocommunications group at TU/e. In October 2006, he joined Philips Research, Eindhoven, The Netherlands. His current interests include wireless communications and signal processing. Dr. Schenk was awarded the 2006 Veder Award by the Dutch Scientific Radio Fund Veder for his contributions in the field of system optimisation for multiple-antenna systems.

He is a member of IEEE, the Royal Institute of Engineers in The Netherlands (KIvI) and he is the chairman of the lecture committee of the Dutch Electronics and Radio Society (NERG).

Erik R. Fledderus received the M.Sc. (cum laude) and Ph.D. degrees in Applied Mathematics from Twente University of Technology, Enschede, The Netherlands, in 1993 and 1997, respectively. From 1997 onwards, he was with KPN Research (now TNO Information and Communication Technology), Leidschendam, The Netherlands, and from 2003 he is part-time professor with the Radiocommunications group of Eindhoven University of Technology in the area of wireless communications networks. His research interests and publications are in the areas of design and simulation of radio networks, smart antennas and propagation modelling. At TNO Information and Communication Technology, Prof. Fledderus is manager of the "Ambient Networks and Services" program.

Peter F. M. Smulders graduated from Eindhoven University of Technology in 1985. In 1985 he joined the Propagation and Electromagnetic Compatibility Department of the Research Neher Laboratories of the Netherlands PTT. During that time he was doing research in the field of compromising emanation from civil data processing equipment. In 1988 he moved to the Eindhoven University of Technology as a staff member of the Telecommunication Division. Next to his lecturing duties he performed a Ph.D. research in the field of 60 GHz broadband wireless LANs. His current work addresses the feasibility of low-cost, low power small sized wireless LAN technology operating in the 60 GHz frequency band to enable unprecedented maximum user data rates in the order of Gbps.

He is senior member of IEEE and his research interest that covers 60 GHz physical and higher layers is reflected in numerous IEEE publications. He was involved in various research projects addressing 60 GHz antennas and interworking (ACTS, MEDIAN) and 60 GHz propagation (MinEZ, Broadband Radio@Hand). Currently, he is also addressing baseband design in the context of 60 GHz radio. As project manager of the SiGi Spot project his future research activities will range from 60 GHz physical layer design to associated network aspects.